frontiers | Frontiers in Mechanical Engineering

TYPE Original Research
PUBLISHED 13 January 2026
DOI 10.3389/fmech.2025.1739706

OPEN ACCESS

EDITED BY
Suvash C. Saha,
University of Technology Sydney, Australia

REVIEWED BY
Muhammet Kaan Yeşilyurt,
Atatürk University, Türkiye
Prashant Saini,
National Renewable Energy Laboratory (DOE), United States

*CORRESPONDENCE
Withada Jedsadaratanachai,
withada.je@kmitl.ac.th

RECEIVED 05 November 2025
REVISED 15 December 2025
ACCEPTED 29 December 2025
PUBLISHED 13 January 2026

CITATION
Boonloi A and Jedsadaratanachai W (2026) Enhancing convective heat transfer coefficient in a circular heat exchanger tube mounted with modified V-orifice (MVO): CFD analysis and correlations.
Front. Mech. Eng. 11:1739706.
doi: 10.3389/fmech.2025.1739706

Enhancing convective heat transfer coefficient in a circular heat exchanger tube mounted with modified V-orifice (MVO): CFD analysis and correlations

Amnart Boonloi[1] and Withada Jedsadaratanachai[2]*

[1]Department of Mechanical Engineering Technology, College of Industrial Technology, King Mongkut's University of Technology North Bangkok, Bangkok, Thailand, [2]Department of Mechanical Engineering, School of Engineering, King Mongkut's Institute of Technology Ladkrabang, Bangkok, Thailand

This study investigates the airflow dynamics and heat transfer (HT) profiles in a circular heat exchanger tube (CHET) mounted with a modified V-orifice (MVO) acting as a turbulator/vortex generator, which is a passive technique to enhance HT. A numerical modeling approach based on the finite volume method using a commercial software package was employed to provide detailed insights into the air flow profile, which is essential for the design of both the turbulator and the CHET system. The MVO is a turbulator derived from the orifice concept, an established engineering device, and has been adapted in combination with a V-shaped structure to effectively generate vortices and enhance HT. Key parameters expected to influence the flow and HT behavior were investigated. These include the ratio of the MVO thickness, b, to the CHET diameter, D (referred to as the blockage ratio, B-R), which was studied in the range of 0.05–0.30, and the ratio of the MVO spacing, P, to the CHET diameter (pitch ratio, P-R), which was considered at values of 1, 1.5, and 2. Attack angles of 30°, 45°, and 60° were examined for both + x and−x flow directions. The study covered turbulent flow conditions corresponding to Reynolds numbers in the range of 3,000–16000, representative of the operating conditions at the CHET inlet. The results indicate that MVO installation in the CHET acts as a flow obstruction, generating a pressure difference that induces vortex formation. These vortices play a key role in modifying the HT behavior, resulting in increased convective HT coefficients. The outcomes are summarized in forms of dimensionless variables. The highest observed HT enhancement reached 9.93 times that of the plain CHET, while the maximum thermal enhancement factor (TEF) was 1.92, obtained at an attack angle of 30°, P-R = 1, B-R = 0.25, in the +x fluid-flow direction at Re = 3,000.

KEYWORDS

heat exchanger, heat transfer enhancement, modified V-orifice, thermal enhancement factor, vortex generator

1 Introduction

Due to the increasing demand for energy in human daily life, it has become essential to establish effective energy management plans, maximize energy utilization, and develop systems and devices with sufficient performance/efficiency to meet this rising demand. It can be observed that many organizations, both governmental and private, have acknowledged this issue and placed importance on collaborative energy management. For instance, the government has provided funding to support research aimed at enhancing the capacity of engineering systems in line with energy management plans. Similarly, the private sector has contributed by supplying various tools for energy utilization testing.

In this research, the team recognized the significance of sustainable energy management and focused on a key system that plays an important role in industry and is closely related to energy consumption—the heat exchanger system. The research began with the development of heat exchanger systems by reviewing previously published studies and selecting one technique for system improvement: the passive technique (the use of vortex generator/turbulator) to enhance the thermal performance of heat exchangers.

In this section, relevant studies are reviewed as follows. Rinik et al. (2025) numerically investigated heat transfer (HT) enhancement in a double-pipe heat exchanger using an elliptical twisted inner pipe combined with convergent conical ring turbulators under turbulent flow conditions (Re = 5,000–26,000). Their results indicated that the full twists generated a strong swirling motion, while the conical rings installed inside the outer pipe acted as passive turbulators that redirected the flow toward the hot fluid in the inner pipe. A maximum performance evaluation criterion (PEC) of approximately 2.3 was reported. Similarly, Li et al. (2024) employed conical rings to enhance the thermal performance of a micro-combustor. Kumar et al. (2023) experimentally evaluated HT and frictional losses in a heat exchanger fitted with perforated conical rings, twisted tapes, and CuO/H_2O nanofluids, observing a maximum thermal–hydraulic performance of about 1.45. Hassan et al. (2022) examined solid and perforated conical rings under turbulent conditions and concluded that the optimal thermal enhancement factor reached 1.2. Alqaed et al. (2024) analyzed turbulent water–copper nanofluid flow in a power-plant heat exchanger fitted with conical ring vortex turbulators. Their results showed that the smallest turbulator length and diameter combined with an inter-turbulator spacing of 145 mm produced the highest frictional entropy generation, while smaller spacings paired with larger turbulator dimensions yielded the lowest friction loss. They further reported that increasing the hole diameter significantly reduced thermal entropy (by 98.7%), frictional entropy (by 72.5%), and total entropy generation (by 98.5%). Ibrahim et al. (2019) performed a computational HT analysis in a circular tube equipped with conical ring turbulators and reported a maximum tube-efficiency enhancement of 1.291, noting that entropy generation increased with Reynolds number across all tested configurations. Kumar et al. (2020) developed empirical correlations for HT and pressure drop in an impinging-jet solar air heater containing internal conical ring vortex generators. The optimal HT efficiency occurred at a relative inner-ring height of 0.110, an inlet-to-ring diameter ratio of 1.7, a ring diameter-to-height ratio of 2.33, a relative X-axis pitch of 5.28, and a relative Y-axis pitch of 3.42. Nakhchi and Esfahani, (2019a), Nakhchi and Esfahani, (2019b) numerically examined turbulent Cu–water nanofluid flow in tubes fitted with perforated conical rings. Their results showed a 278.2% increase in HT compared with a smooth tube and a maximum thermal performance factor of 1.10 at Re = 5,000. However, increasing the number of holes from 4 to 10 reduced the Nusselt number by up to 35.48%, while the highest thermal performance factor obtained was 1.241. Anvari et al. (2014), Anvari et al. (2011) conducted combined experimental and numerical investigations of tubes fitted with special conical ring vortex generators. They reported that using water instead of air as the working fluid resulted in reduced HT enhancement efficiency. Nonetheless, the addition of turbulators increased the Nusselt number by up to 521% for diverging conical rings and 355% for converging rings, albeit with a substantial increase in pressure drop. Sheikholeslami et al. (2016) studied turbulent air-to-water flow in a double-pipe heat exchanger equipped with conical rings. Their results showed that the friction factor decreased with increasing open-area ratio, pitch ratio, and Reynolds number, while the Nusselt number decreased with open-area ratio and pitch ratio but increased with Reynolds number. They further concluded that thermo-hydraulic performance improved with larger conical angles in direct conical-ring arrays. Mohammed et al. (2019) analyzed two-phase forced convection of nanofluids in circular tubes fitted with convergent and divergent conical ring inserts. The divergent-ring configuration provided the best PEC, yielding up to 365% enhancement at equal pumping power. They also demonstrated that the two-phase mixture model predicted HT behavior more accurately than the single-phase model when validated against experimental and numerical data. Sripattanapipat et al. (Sripattan et al., 2016) numerically examined HT in a tube equipped with hexagonal conical-ring inserts and found that V-shaped hexagonal rings produced significantly higher HT compared with both the smooth tube and the reference configuration, while simultaneously reducing the friction factor. Finally, Kongkaitpaiboon et al. (2010a) experimentally studied HT and turbulent-flow friction in tubes fitted with perforated conical rings, reporting a maximum thermal performance factor of approximately 0.92 at a pitch ratio of 4 and Re = 4,000. Beyond conical rings, other passive vortex generators—such as twisted tapes (Bizuneh et al., 2025; Kumar and Afzal, 2025; V P et al., 2025; Abajja et al., 2023; Bhattacharyya et al., 2025; Ghazanfari et al., 2025), baffles/ribs (Salhi et al., 2025; Wang et al., 2025; Zhan et al., 2025; Li et al., 2025; Bennour et al., 2025), winglets (Feng et al., 2024; Suchatawat et al., 2025; İĞCİ, 2025; Tian et al., 2024; Majmader and Hasan, 2024), helical wire coils (Saini et al., 2024a), and X-grid static mixers (Saini et al., 2024b)—are also widely used to enhance convective HT and improve overall heat exchanger performance.

In this research, the team employed a well-known engineering device, the orifice. When compared with conventional vortex generators available in the market, the orifice was found to share a similarity with the conical ring. This was further developed in combination with a configuration that has attracted significant attention due to its relatively high performance in enhancing HT, namely, the V-shape. From previous studies, it has been reported that V-baffles and V-ribs can effectively enhance HT rates in various types of heat exchanger tubes.

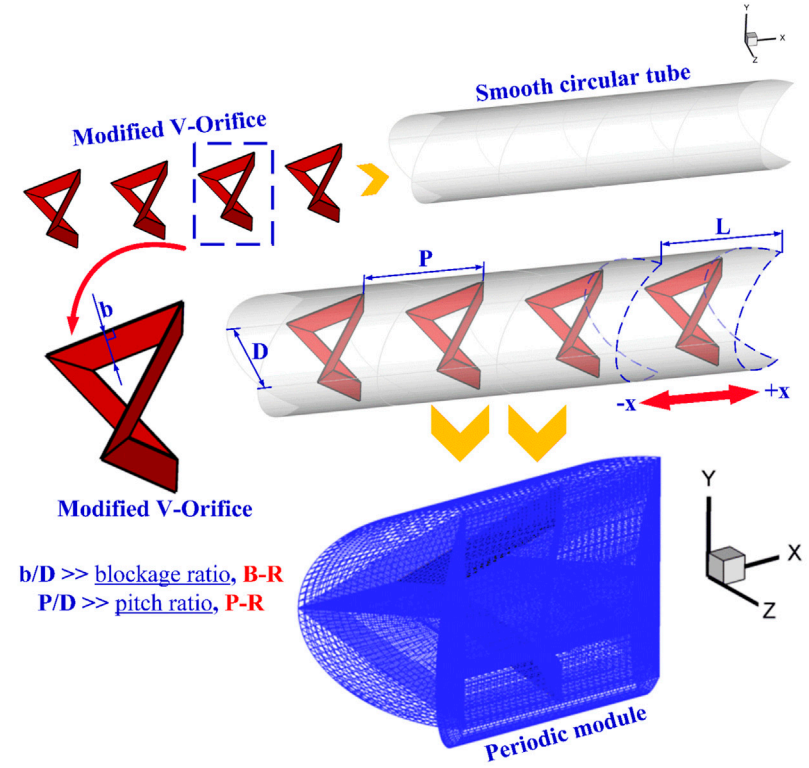

(a)

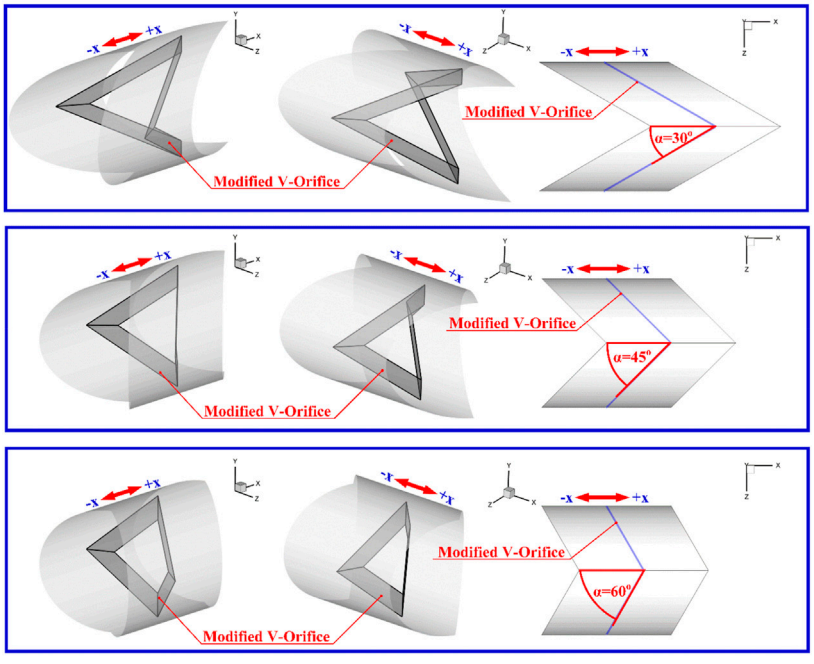

(b)

FIGURE 1
(a) Computational model for a circular tube heat exchanger inserted with MVO and **(b)** periodic module description.

For this study, the vortex generator was referred to as the modified V-orifice (MVO) and was applied to a circular heat exchanger tube (CHET), which is one of the most commonly used heat exchanger systems in industry. The research investigated several parameters, including size, arrangement, and flow direction, within the turbulent flow regime that encompasses

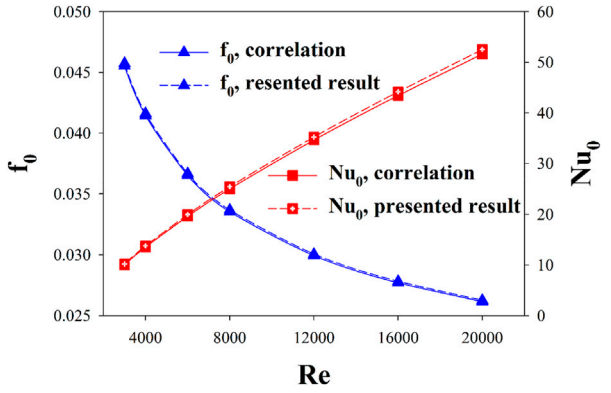

FIGURE 2
Smooth tube validation.

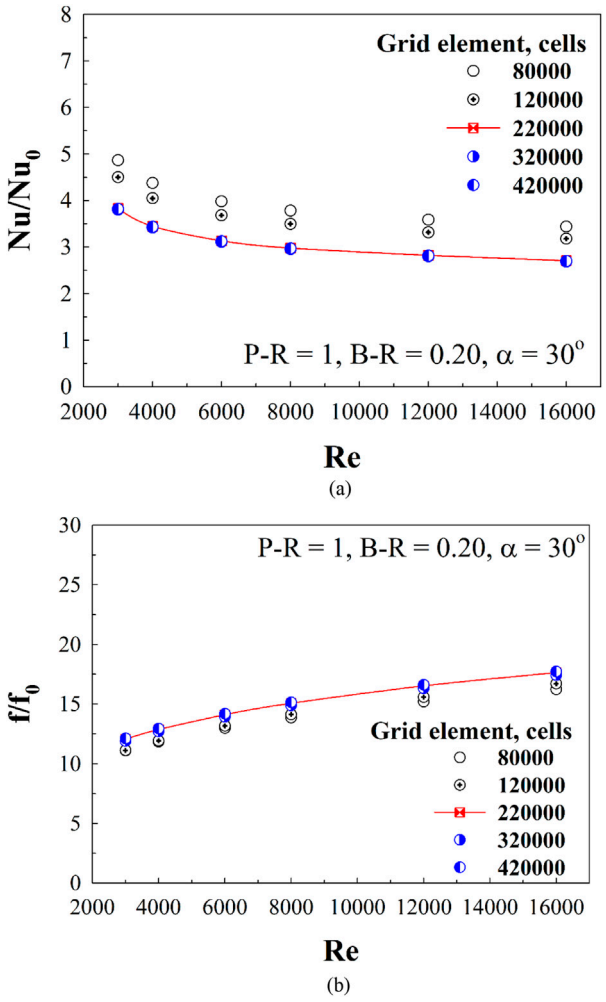

FIGURE 3
Grid independence for **(a)** Nu/Nu_0 and **(b)** f/f_0 of the numerical model at P-R = 1, B-R = 0.20 and α = 30°.

many engineering applications. The present work employed numerical modeling using a reliable and academically recognized software. This method enables the explanation of flow and HT behaviors occurring in the system and provides a significant guideline for the future improvement of heat exchanger and thermal systems (Zhang et al., 2025). Furthermore, it allows for resource and cost savings in the research process.

2 Numerical model of the CHET mounted with MVO and MVO configurations

In this section, the details of the model investigated in this study are described, including the parameters and variables employed in the research. The heat exchanger system used in the present research is a circular heat exchanger tube (CHET). The CHET are widely used in many industrial applications due to their ability to withstand internal pressure uniformly in all directions, making them suitable for both gases and liquids. The CHET diameter, denoted as D, is 0.05 m. The turbulence generator employed in this study was developed from an orifice plate, a device commonly used for flow rate measurement in engineering, combined with a geometric feature often adopted for turbulence generation—the V-shape—commonly used in ribs and baffles, referred to as V-rib and V-baffle, respectively. This concept was modified to create a vortex generator in the present study, termed the modified V-orifice (MVO). The thickness of the MVO plate is symbolized as b. The ratio of b to the CHET diameter D, expressed as b/D, is called the blockage ratio (B-R). For this study, the B-R values range from 0.05 to 0.30. The axial distance between MVO plates is denoted as P. The ratio of P to the CHET diameter D, expressed as P/D, is called the pitch ratio (P-R), with values ranging from 1 to 2. Since the CHET considered in this study represents a long industrial tube, the model is designed with periodic inlet and outlet boundary conditions for both fluid flow and HT. The periodic module length is denoted as L, with L = D, 1.5D and 2D for P-R values of 1, 1.5, and 2, respectively. Both forward and backward flow directions along the x-axis are considered. Figure 1a illustrates the details of the computational model for this study, while Figure 1b presents the MVO configurations with different attack angles. The attack angles considered are 30°, 45° and 60°. The investigation focuses on turbulent flow conditions (based on the entry conditions of the numerical model), with Reynolds numbers in the range of 3,000–16,000, covering the operational range of various industrial heat exchangers. The numerical model was developed using a non-uniform structured grid, in which a refined mesh was employed near the heat-transfer wall. The resulting y^+ values were maintained at approximately 1 for all cases, consistent with recommended numerical modeling practices to ensure accurate and reliable predictions.

3 Numerical setting, initial and boundary conditions

The computational configuration of the CHET equipped with MVO inserts is established with the boundary conditions as

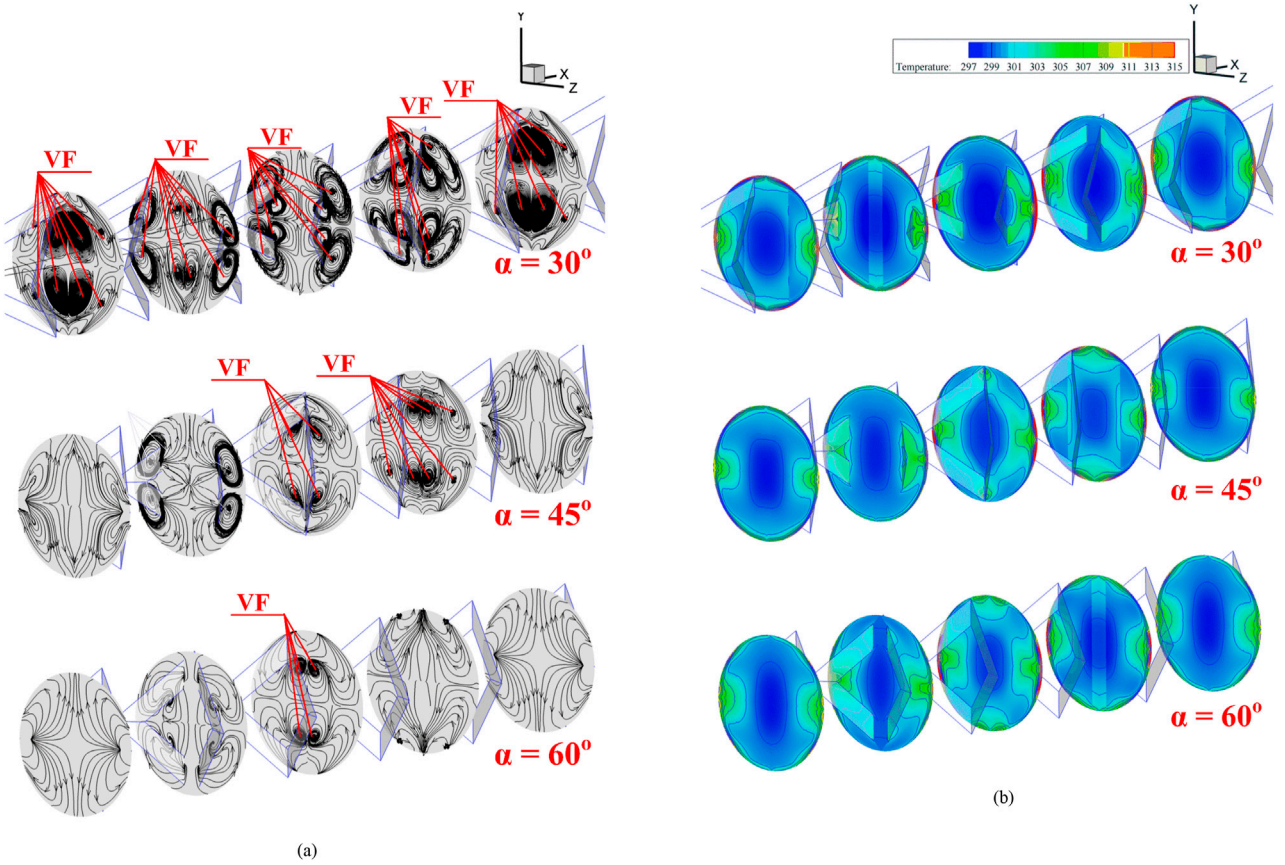

FIGURE 4
Mechanisms in the tested tube for **(a)** flow configuration (streamlines in y-z planes) and **(b)** HT characteristics (temperature in y-z planes).

follows. Periodic boundary conditions are imposed at both the inlet and outlet sections for the fluid flow and thermal domains. Periodic flow and heat transfer were employed to represent a long-tube heat exchanger typically found in industrial applications, where the tube length is generally more than ten times the hydraulic diameter or the inlet diameter of the tube. Under these conditions, the flow and heat transfer are considered fully developed. A uniform heat flux of 600 W/m^2 is applied to the CHET surface, whereas the MVO plates are treated as adiabatic surface, with no heat flux (0 W/m^2).

The assumptions and initial conditions adopted in this research are outlined as follows:

- Air is considered the working fluid, entering at 300 K, with both flow and HT at the CHET inlet assumed to be fully developed.
- Since the temperature rise of the tested fluid during the simulation does not exceed 20 °C/K, its thermophysical properties are regarded as constant.
- Flow and HT are modeled as steady-state and three-dimensional.
- The HT analysis accounts solely for forced convection, while natural convection and radiation are disregarded as negligible.
- Effects of body forces and viscous dissipation are also omitted.

4 Mathematical foundation

Based on the details of the investigation stated above, the governing equations used in the current study are as follows (Cengel and Ghajar, 2015):

The continuity equation employed in this research is presented in Equation 1. The flow and HT phenomena are governed by the momentum and energy equations, which are formulated in Equations 2, 3, respectively.

$$\frac{\partial}{\partial x_i}\left(\rho u_i\right) = 0 \tag{1}$$

$$\frac{\partial}{\partial x_i}\left(\rho u_i u_j\right) = -\frac{\partial p}{\partial x_i} + \frac{\partial}{\partial x_j}\left[\mu\left(\frac{\partial u_i}{\partial x_j}\right) - \rho\overline{u_i' u_j'}\right] \tag{2}$$

$$\frac{\partial}{\partial x_i}\left(\rho u_i T\right) = \frac{\partial}{\partial x_j}\left[\left(\Gamma + \Gamma_t\right)\frac{\partial T}{\partial x_j}\right] \tag{3}$$

Γ and Γ_t denote the molecular and turbulent thermal diffusivities, respectively, and are calculated as Equation 4:

$$\Gamma = \mu / Pr \text{ and } \Gamma_t = \mu_t / Pr_t \tag{4}$$

The Reynolds-averaged approach to turbulence modeling requires that the Reynolds, $-\rho\overline{u_i' u_j'}$ in Equation 2, be modeled. Equation 5 presents the Boussinesq hypothesis, which relates the Reynolds stresses to the mean velocity gradients:

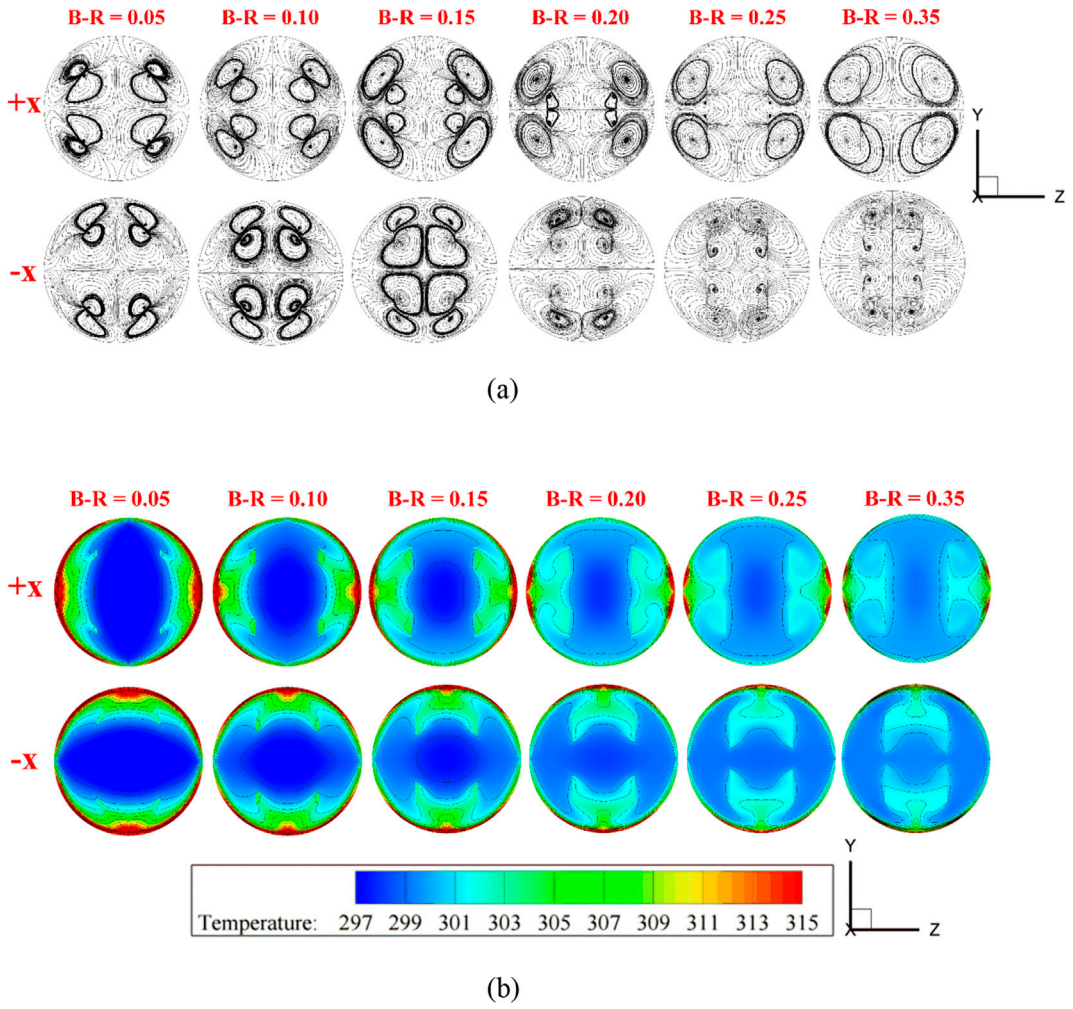

FIGURE 5
Flow and HT profiles in the tested tube at various B-R of α = 30°, Re = 4,000 and P-R = 1 for **(a)** streamlines in y-z planes and **(b)** air temperature distributions in y-z planes.

$$-\rho\overline{u_i'u_j'} = \mu_t\left(\frac{\partial u_i}{\partial x_j}+\frac{\partial u_j}{\partial x_i}\right)-\frac{2}{3}\left(\rho k+\mu_t\frac{\partial u_i}{\partial x_i}\right)\delta_{ij} \quad (5)$$

Here, the turbulent kinetic energy, k, is defined by $k = (\overline{u_i'u_i'})/2$ and δ_{ij} is a Kronecker delta. A key advantage of the Boussinesq approach lies in its relatively low computational cost associated with the calculation of the turbulent viscosity, μ_t, as given by $\mu_t = \rho C_\mu k^2/\varepsilon$. The RNG k–ε model is an example of the two-equation models that use the Boussinesq hypothesis. It is derived from the instantaneous Navier–Stokes equations using the renormalization group (RNG) method. The steady-state transport equations are expressed as Equations 6, 7:

$$\frac{\partial}{\partial x_i}(\rho k u_i) = \frac{\partial}{\partial x_j}\left(\alpha_k \mu_{eff}\frac{\partial k}{\partial x_j}\right)+G_k-\rho\varepsilon \quad (6)$$

$$\frac{\partial}{\partial x_i}(\rho\varepsilon u_i) = \frac{\partial}{\partial x_j}\left(\alpha_k \mu_{eff}\frac{\partial \varepsilon}{\partial x_j}\right)+C_{1\varepsilon}\frac{\varepsilon}{k}G_k-C_{2\varepsilon}\rho\frac{\varepsilon^2}{k}-R_\varepsilon \quad (7)$$

Here, α_k represents the inverse effective Prandtl number for k, while α_ε stands for ε. $C_{1\varepsilon}$ and $C_{2\varepsilon}$ remain constants. The effective viscosity, μ_{eff}, is expressed as Equation 8:

$$\mu_{eff} = \mu+\mu_t = \mu+\rho C_\mu\frac{k^2}{\varepsilon} \quad (8)$$

The governing equations were discretized using the QUICK scheme to ensure higher-order accuracy in predicting convection-dominated flows. The finite volume method was applied for spatial discretization across the computational domain. Pressure–velocity coupling was resolved using the SIMPLE algorithm, with under-relaxation factors adjusted to maintain numerical stability throughout the iteration process. All simulations were carried out using the commercial CFD solver ANSYS Fluent. Convergence was assumed when the normalized residuals for the continuity, momentum, and turbulence-related variables fell below 10^{-5}, while a more stringent criterion of 10^{-9} was imposed on the energy equation to ensure accurate thermal-field prediction.

The fluid velocity is characterized by the Reynolds number, calculated according to Equation 9. The pressure drop within the heat exchanger system is represented by the friction factor, following Equation 10. Heat transfer is quantified through the local and average Nusselt numbers, as presented in Equations 11,12, respectively. The

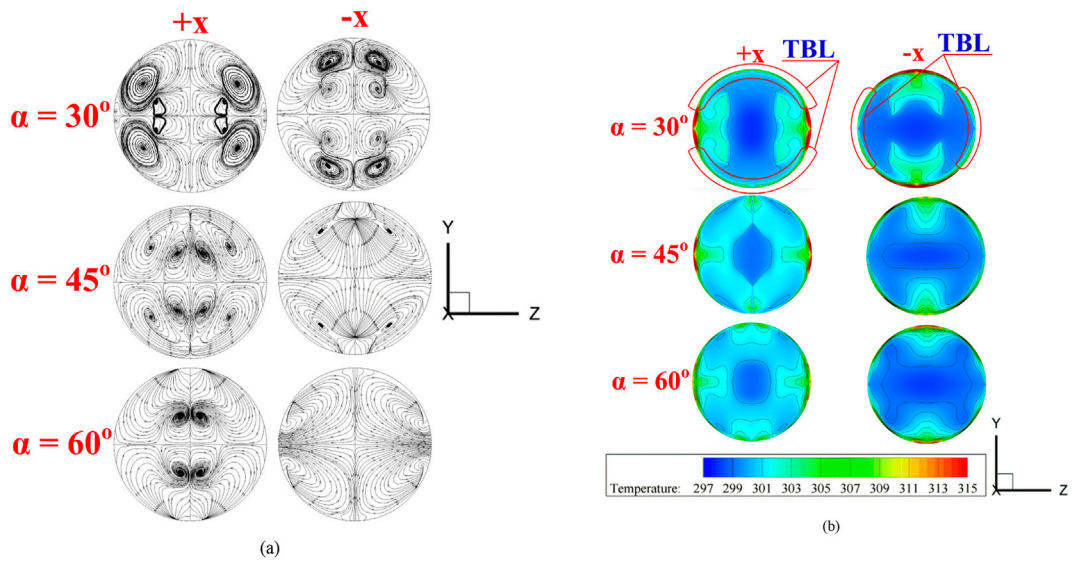

FIGURE 6
Flow and HT profiles in the tested tube at various attack angles of B-R = 0.15, Re = 4,000 and P-R = 1 for **(a)** streamlines in y-z planes and **(b)** air temperature distributions in y-z planes.

performance of heat transfer enhancement, expressed as the thermal enhancement factor (TEF), can be determined using Equation 13.

$$Re = \frac{\rho \bar{u} D_h}{\mu} \tag{9}$$

$$f = \frac{(\Delta p/L)D_h}{1/2\rho\bar{u}^2} \tag{10}$$

$$Nu_x = \frac{h_x D_h}{k} \tag{11}$$

$$Nu = \frac{1}{A}\int Nu_x dA \tag{12}$$

$$TEF = \frac{h}{h_0}\Big|_{pp} = \frac{Nu}{Nu_0}\Big|_{pp} = \frac{(Nu/Nu_0)}{(f/f_0)^{1/3}} \tag{13}$$

Here, Nu_0 and f_0 represent the Nusselt number and friction factor, respectively, for the smooth CHET.

5 Numerical-model validation

Model validation represents a fundamental step in numerical simulations. In the present research, the validation process for turbulent flow conditions is divided into three stages: (1) assessment with a smooth CHET, (2) evaluation of mesh independence to identify the suitable grid resolution, and (3) comparison of the numerical predictions with published works (Kongkaitpaiboon et al., 2010b; Jedsadaratanachai and Boonloi, 2017).

5.1 Smooth CHET validation

The Nusselt number and friction factor predicted by the developed numerical model for a smooth CHET were evaluated against values obtained from a standard empirical correlation (Cengel and Ghajar, 2015) under turbulent flow conditions. The comparison revealed discrepancies of 1.7% in the Nusselt number and 4.2% in the friction factor (see Figure 2). Such minor differences confirm the strong agreement and demonstrate the reliability of the numerical model.

5.2 Grid independence

A grid independence test was carried out for the CHET with the MVO (P-R = 1, B-R = 0.20, α = 30°) using five mesh densities: 80,000; 120,000; 220,000; 320,000; and 420,000 cells. The numerical results pointed out that refining the mesh from 220,000 to 420,000 elements produced negligible variations in the Nusselt number and friction factor across the entire Reynolds number range (see Figure 3). Considering both accuracy and computational efficiency, a grid size of about 220,000 elements was chosen for the subsequent simulations. For models with extended computational domains, the number of mesh elements was proportionally scaled to preserve quality and consistency of the solutions.

5.3 Comparison of the experimental results

As no prior studies have introduced a vortex generator identical to the MVO proposed herein, the present model was validated by comparison with earlier investigations (Kongkaitpaiboon et al., 2010b; Jedsadaratanachai and Boonloi, 2017), which examined a circular ring (Kongkaitpaiboon et al., 2010b) and a V-orifice (Jedsadaratanachai and Boonloi, 2017) mounted inside a CHET. The reference (Kongkaitpaiboon et al., 2010b) corresponds to an experimental study, whereas reference (Jedsadaratanachai and Boonloi, 2017) pertains to a numerical investigation. Both the present study and the work cited in reference (Jedsadaratanachai

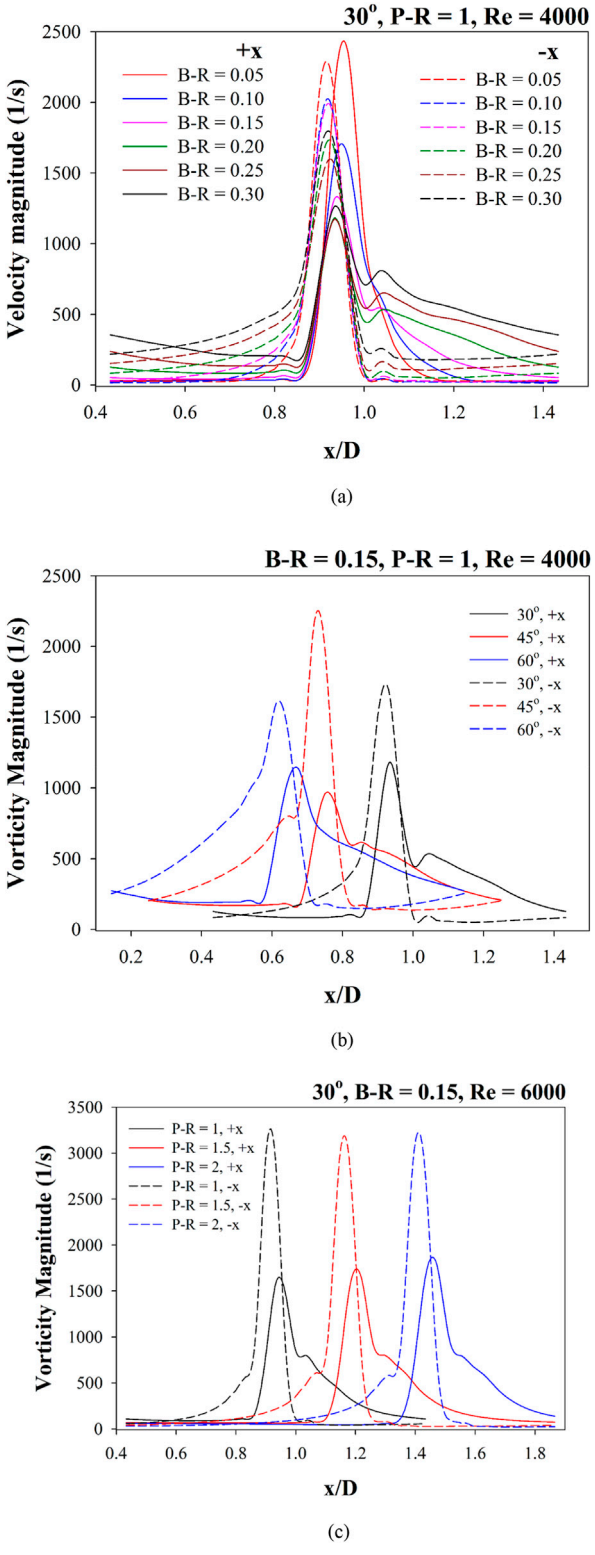

FIGURE 7
Velocity magnitude vs. x/D for **(a)** various B-R, **(b)** various attack angles and **(c)** various P-R.

and Boonloi, 2017) adopt comparable numerical configurations, including the application of the SIMPLE algorithm, the k–ε turbulence model, and the enhanced wall treatment approach. The validation considered both the Nusselt number and friction factor. Results showed that the present model differed from (Kongkaitpaiboon et al., 2010b) by about 6% in the Nusselt number and 15% in the friction factor, whereas the deviations relative to (Jedsadaratanachai and Boonloi, 2017) were negligible, only 0.02% for both parameters. Consistent with previous studies, the differences in Nu and f follow the same trend: the variation in Nu is generally small, whereas the friction factor shows relatively larger differences. Nevertheless, the values remain within an acceptable range, and no intersection of the plotted curves is observed. These outcomes confirm that the developed model is sufficiently accurate for predicting fluid flow and HT in a CHET equipped with the proposed MVO.

6 Numerical result and discussion

The numerical results of the current research are presented in three important parts. The first part describes the fluid flow structure and thermal characteristics in the CHET equipped with MVOs, illustrated through streamlines along different axes, temperature contours, and Nusselt number contours, among others. The second part summarizes the HT rate, pressure loss, and thermal performance in the form of correlation graphs. The HT rate is expressed as the ratio Nu/Nu0, while the pressure loss is presented as f/f_0. The thermal performance is represented by the thermal enhancement factor (TEF), which evaluates the increase in HT achieved by installing MVOs in the CHET under the same pumping power conditions. The final part synthesizes the results obtained from the present study to develop TEF contours in relation to other variables, as well as to present the correlation equations derived from this research. Both aspects can serve as practical guidelines for designing heat exchanger systems incorporating MVOs for real industrial applications.

6.1 Flow and HT behavior

The primary flow structure of interest in the CHET with the installation of MVO is the vortex flow. The verification of vortex formation within the heat exchanger system can be assessed from the cross-sectional vortex flow patterns, as illustrated in Figure 4a. In this figure, five cross-sectional planes are created, distributed along one module of the model. It is observed that, in all studied cases, the incorporation of MVO induces vortex flow in the CHET. The vortex cores, represented by VF, indicate that at an impingement angle of 30°, VF can be clearly observed across all constructed planes. In contrast, for impingement angles of 45° and 60°, VF is only observed in certain planes.

The vortex flow structures generated within the CHET play a decisive role in determining its thermal behavior. Since the turbulent kinetic energy (TKE) and temperature contours exhibit consistent trends in representing vortex strength and mixing intensity, only the temperature contours are presented in this study to maintain conciseness. Figure 4b shows the temperature distribution on the transverse plane along the test section of the CHET.

In a conventional CHET without vortex generators, the temperature field is characterized by a low-temperature core region surrounded by a high-temperature zone near the heated wall, forming a relatively thick thermal boundary layer. With the installation of multiple vortex generators (MVOs), the induced vortical motion

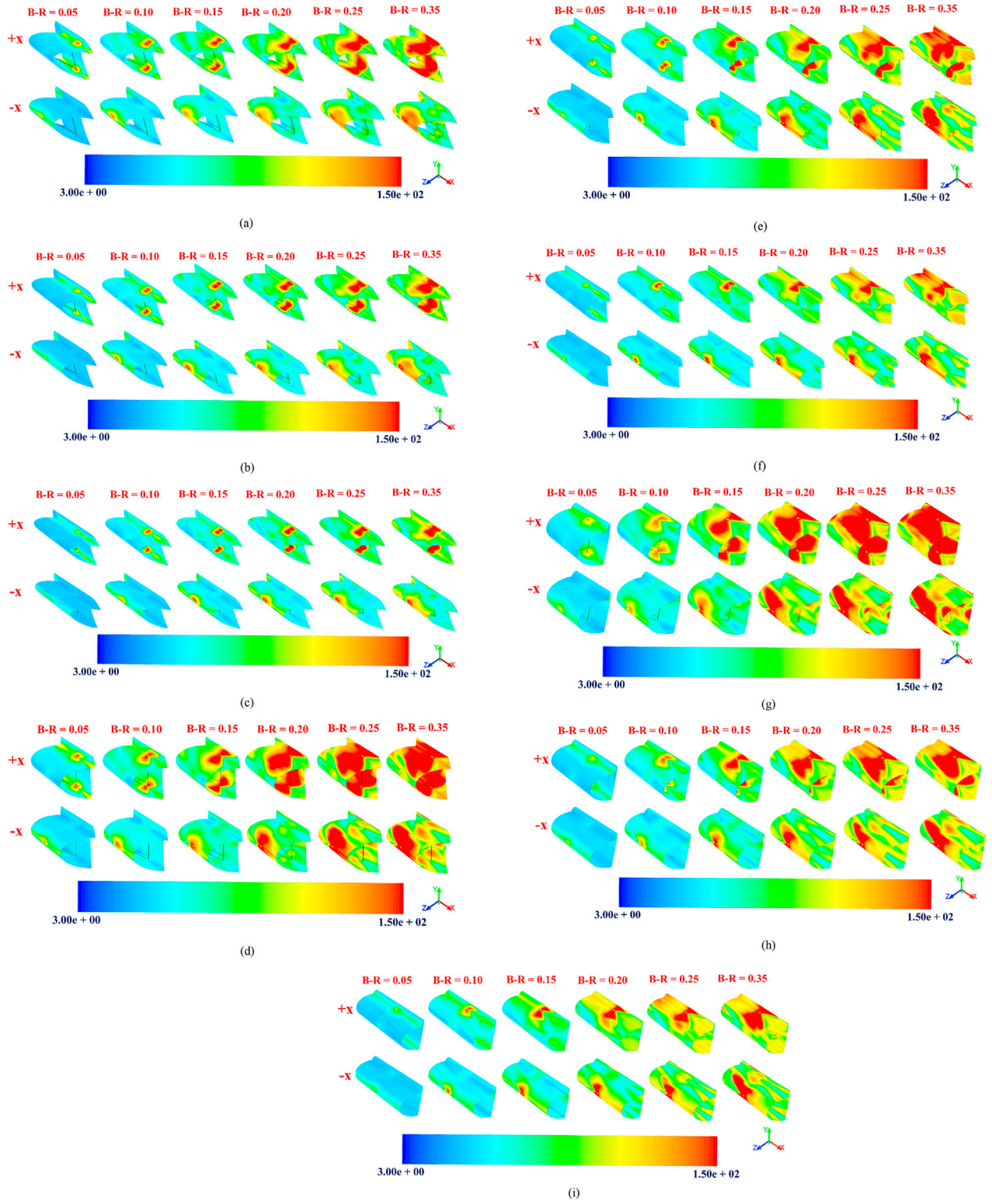

FIGURE 8
Nusselt number contours on the tube wall of the tested tube inserted with MVO at Re = 6,000 for **(a)** 30°, P-R = 1, **(b)** 30°, P-R = 1.5, **(c)** 30°, P-R = 2, **(d)** 45°, P-R = 1, **(e)** 45°, P-R = 1.5, **(f)** 45°, P-R = 2, **(g)** 60°, P-R = 1, **(h)** 60°, P-R = 1.5, **(i)** 60°, P-R = 2.

substantially alters this distribution. The low-temperature fluid spreads outward from the core and penetrates adjacent layers, while the near-wall high-temperature region becomes noticeably thinner or locally indistinct. The thinning of the high-temperature layer signifies disruption of the thermal boundary layer, whereas the outward transport of low-temperature fluid reflects enhanced mixing.

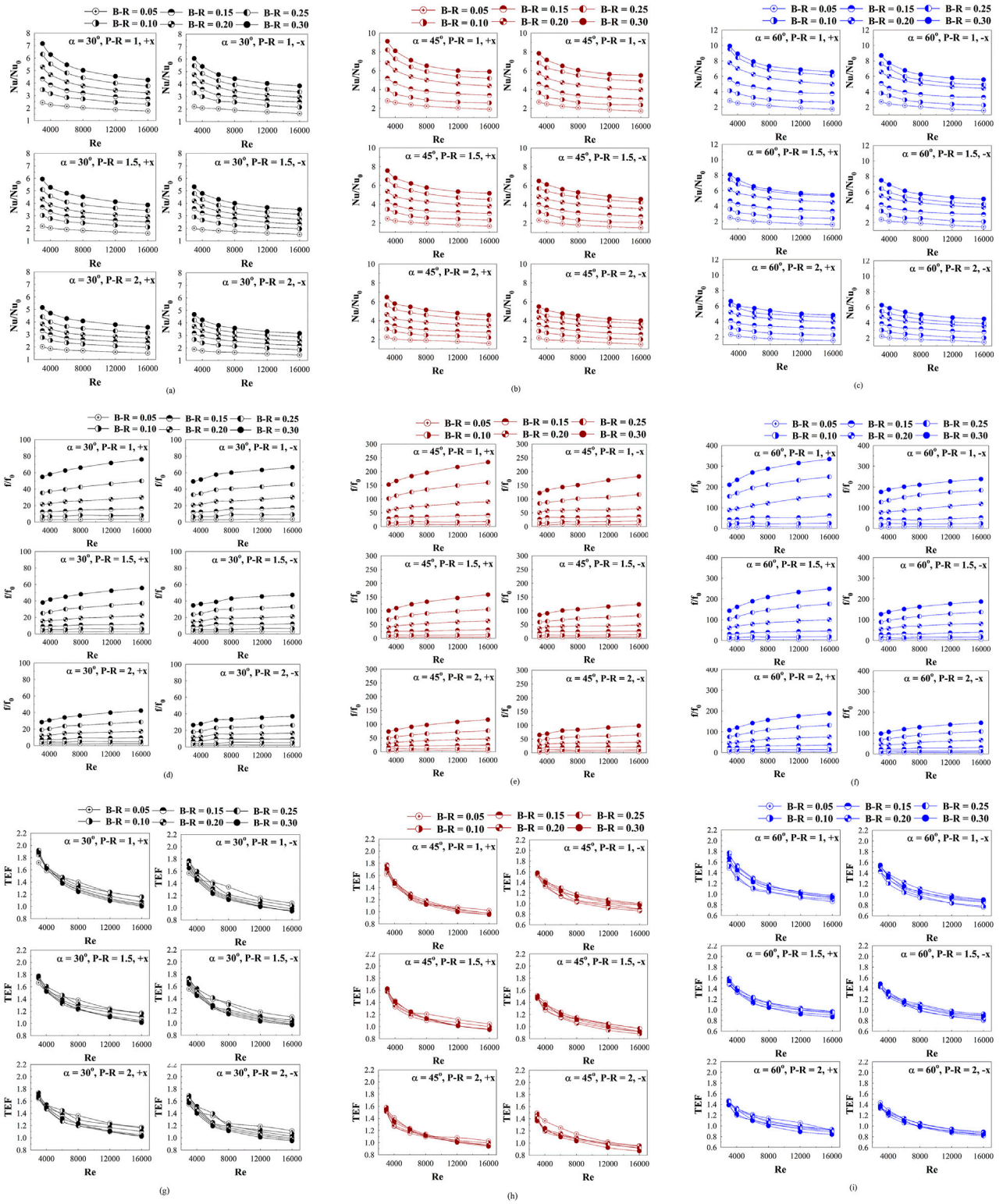

FIGURE 9
Performance evaluations of the tested tube inserted with MVO for **(a)** 30°, Nu/Nu_0 vs. Re, **(b)** 45°, Nu/Nu_0 vs. Re, **(c)** 60°, Nu/Nu_0 vs. Re, **(d)** 30°, f/f_0 vs. Re, **(e)** 45°, f/f_0 vs. Re, **(f)** 60°, f/f_0 vs. Re, **(g)** 30°, TEF vs. Re, **(h)** 45°, TEF vs. Re, **(i)** 60°, TEF vs. Re.

These characteristics are consistently observed in all cases with MVO installation and collectively contribute to increased convective heat transfer within the CHET.

Figure 5a presents the streamline patterns on the transverse plane for different B–R values under both + x and −x flow directions. Vortex structures are observed in all cases, although

TABLE 1 Nu/Nu_0, f/f_0 and TEF in the CHET equipped with the MVO at various cases.

Attack angle	Flow direction	P-R	Nu/Nu_0	f/f_0	TEF	B-R that performs maximum TEF
30°	+x	1	1.76–7.16	2.88–76.08	1.92	0.25
		1.5	1.61–5.95	2.24–55.66	1.78	0.10
		2	1.51–5.15	1.89–42.38	1.74	0.10
	-x	1	1.64–6.05	2.75–66.63	1.77	0.10–0.15
		1.5	1.52–5.33	2.15–47.35	1.73	0.15
		2	1.49–4.68	1.84–37.09	1.69	0.10
45°	+x	1	1.89–9.13	5.14–234.15	1.78	0.20
		1.5	1.67–7.57	3.73–158.98	1.63	0.30
		2	1.57–6.48	2.97–116.56	1.58	0.10
	-x	1	1.69–7.84	4.98–182.23	1.58	0.30
		1.5	1.51–6.50	3.70–123.44	1.51	0.10
		2	1.48–5.49	2.99–98.02	1.50	0.05
60°	+x	1	1.73–9.93	6.98–334.45	1.77	0.25
		1.5	1.60–8.07	4.51–249.23	1.59	0.25
		2	1.53–6.62	3.82–188.21	1.48	0.05
	-x	1	1.56–8.69	6.79–238.50	1.55	0.30
		1.5	1.45–7.48	4.85–187.61	1.49	0.30
		2	1.48–6.26	3.82–149.79	1.44	0.05

the number and spatial distribution of vortex cores vary with B–R. Increasing the B–R leads to more pronounced vortices, indicating stronger secondary flow development. The corresponding temperature contours in Figure 5b further demonstrate persistent boundary-layer disturbance and enhanced mixing for all B–R values. For a given flow direction, the locations of boundary-layer disruption remain unchanged, while the extent of disturbance and mixing intensity increase with increasing B–R. This behavior is attributed to the MVO acting as a flow obstruction, which generates a pressure difference between upstream and downstream regions. A higher B–R results in greater flow blockage, producing a larger pressure gradient and stronger vortical motion, thereby promoting more effective thermal boundary-layer thinning and mixing.

The influence of attack angle on the flow structure is illustrated in Figure 6a. Variations in flow incidence significantly modify the spatial locations of vortex formation and boundary-layer disturbance, as further confirmed by the corresponding temperature contours shown in Figure 6b.

Figure 7a shows the axial variation of velocity magnitude (x/D) at an attack angle of 30°, with P–R = 1 and Re = 4,000, for different B–R values and both flow directions. Regardless of the B–R, the velocity magnitude follows a similar axial trend, with peak values consistently occurring at x/D ≈ 0.9–1.0. This suggests that the downstream flow acceleration is primarily governed by the overall flow configuration rather than the blockage ratio. The effects of attack angle and P–R on the velocity magnitude are further illustrated in Figures 7b,c. While the velocity profiles retain similar shapes for cases with the same flow direction, the −x flow direction consistently exhibits higher peak velocities, indicating stronger local acceleration and flow impingement, which directly favor heat transfer enhancement.

Figure 8 presents the Nusselt number contours on the CHET surface. Increasing the B–R and decreasing the P–R result in higher local Nusselt numbers, reflecting improved heat transfer performance. This enhancement is evident from the expansion of high-Nusselt regions, which correspond to zones of flow impingement and pronounced boundary-layer disturbance. For a given flow direction, the locations of these regions remain consistent. Specifically, for the +x flow direction, boundary-layer disruption occurs mainly on the upper and lower tube surfaces, whereas for the −x flow direction, it is concentrated along the left and right walls of the CHET. These distributions agree well with the flow structures identified in Figure 6b, confirming the close relationship between vortex-induced impingement and local heat transfer augmentation.

In summary, heat transfer enhancement in the CHET equipped with MVOs is governed by the vortex flow structures generated downstream of the orifices. The induced vortices disrupt and thin the thermal boundary layer while promoting intensive mixing between the low-temperature core fluid and the high-temperature near-wall fluid. Variations in B–R, P–R, attack angle, and flow direction modulate the strength and spatial distribution of these vortices, with higher B–R and lower P–R producing stronger pressure gradients, more energetic vortex cores, and greater boundary-layer disturbance. These flow characteristics are consistent with the observed velocity and streamline patterns,

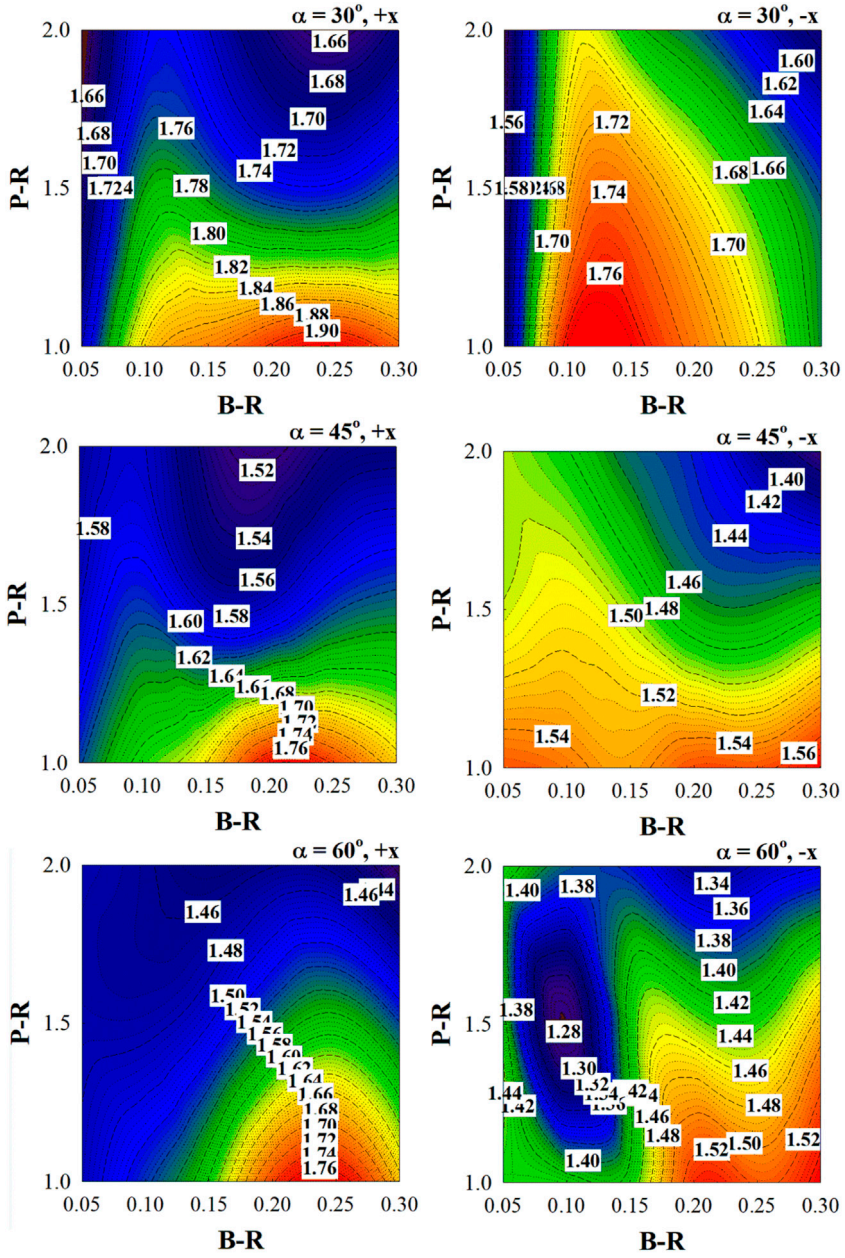

FIGURE 10
TEF contours at various cases for Re = 3,000.

which reveal accelerated flow and intensified mixing near the MVOs. Consequently, regions of elevated Nusselt number coincide with zones of vortex-induced boundary-layer disruption, confirming that the enhancement in thermal performance primarily originates from vortex-driven mixing mechanisms.

6.2 Performance evaluation

The presentation and analysis of data using contours and streamlines, as discussed in the previous section, are insufficient to determine which case provides higher or lower HT rates, pressure drop, or overall thermal performance. Therefore, this section summarizes the thermal performance in terms of the averaged Nusselt number, friction factor, and TEF, which are dimensionless parameters and convenient for comparison among different cases and systems. Figures 9a–c illustrate the relationship between Nu/Nu_0 and Re at various B-R and P-R values for attack angles of 30°, 45°, and 60°, respectively. The results show that Nu/Nu_0 tends to decrease as Re increases. A significant reduction in Nu/Nu_0 is observed in the range of Re = 4,000–8,000, followed by a gradual decline approaching a nearly constant level for Re > 8,000. As discussed earlier regarding the system behavior, vortex strength increases with higher B-R and lower P-R. Consequently, Nu/Nu_0 increases with increasing B-R and decreasing P-R. At P-R = 1–1.5, the Nu/Nu_0 values for the +x flow direction are noticeably higher

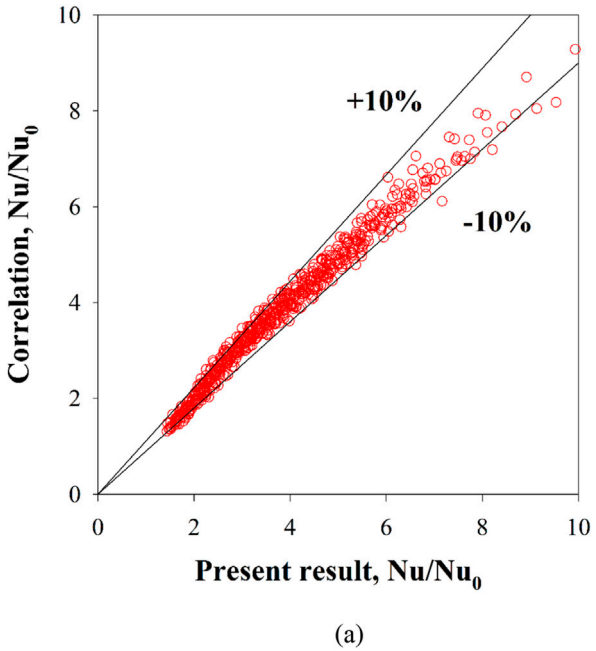

FIGURE 11
Correlation data vs. present results for **(a)** Nu/Nu_0 and **(b)** f/f_0.

than those for the–x direction, whereas at P-R = 2, the Nu/Nu_0 values for both flow directions are nearly identical.

Figures 9d–f illustrate the relationship between f/f_0 and Re at various B-R, P-R, and flow directions for attack angles of 30°, 45°, and 60°, respectively. The results show that f/f_0 increases with increasing Re. This trend is consistent with the flow and HT behavior previously discussed, where higher B-R and lower P-R lead to larger f/f_0 values. The increase in f/f_0 can be attributed to the fact that larger B-R values correspond to a greater flow blockage ratio, which intensifies the pressure difference across the MVO. This pressure difference induces stronger vortices, which in turn enhance boundary-layer disturbance. Although this mechanism improves fluid mixing and promotes higher HT rates, it also increases flow resistance, thereby raising the friction factor.

Furthermore, the observation that f/f_0 values are consistently higher in the +x flow direction compared to the–x direction suggests that flow incidence plays a critical role in determining the pressure loss characteristics of the system. The asymmetry between the two flow directions indicates that the orientation of vortex generation alters the local flow impingement and separation patterns, thereby influencing the pressure drop behavior. These findings highlight the inherent trade-off between HT enhancement and pressure loss when using MVOs, emphasizing the need to evaluate overall thermal performance rather than HT characteristics alone.

Figures 9g–i illustrate the relationship between TEF and Re at various B-R, P-R, and flow directions for attack angles of 30°, 45°, and 60°, respectively. The TEF represents the combined effects of flow restructuring and the pressure-loss penalty introduced by the vortex-generating elements. Higher TEF values are typically associated with strong and stable longitudinal vortices that enhance fluid mixing and effectively disrupt the thermal boundary layer, thereby increasing the Nusselt number without causing an excessive rise in frictional resistance. Favorable flow features—such as near-wall flow acceleration, periodic reattachment, and well-controlled separation zones—further enhance local heat transfer and contribute to improved thermal performance. In contrast, weak or rapidly decaying vortices, overly large recirculation zones, or significant pressure drops relative to the achieved heat-transfer enhancement result in reduced TEF. As the Reynolds number increases, heat-transfer augmentation generally becomes more pronounced; however, the friction factor commonly increases at an even greater rate, causing TEF to gradually decrease unless the geometry can sustain coherent vortex structures. Overall, high TEF values are achieved when the induced vortices effectively strengthen near-wall transport while maintaining a balanced pressure-loss profile. A consistent trend is observed across all cases, showing that TEF decreases with increasing Re. The summarized values of Nu/Nu_0, f/f_0, and TEF are provided in Table 1.

From the summarized table, it is observed that an attack angle of 60° yields the highest Nu/Nu_0 and f/f_0 values compared to the other attack angles, while an attack angle of 45° provides higher Nu/Nu_0 and f/f_0 than that of 30°. The–x flow direction results in lower HT rates than the +x direction but contributes to a reduction in pressure drop within the CHET. When considering the overall effectiveness of MVO installation, expressed in terms of the TEF or the HT improvement at the same pumping power, the highest TEF obtained in this study is 1.92. This maximum occurs at an attack angle of 30°, in the +x flow direction, with P-R = 1 and B-R = 0.25. Therefore, based on TEF, this configuration is recommended for practical applications in industrial heat exchanger systems.

6.3 TEF contours and correlations

Figure 10 presents the TEF contours at various B-R, P-R, attack angles, and flow directions. For the +x flow direction, the highest TEF is achieved at P-R = 1, with the recommended B-R range between 0.20 and 0.25. For the–x flow direction, at an attack angle of 30°, the recommended configuration is P-R = 1 with B-R in the range of

0.10–0.15. At an attack angle of 45°, TEF values are relatively similar for all B-R values when P-R = 1. For an attack angle of 60°, the recommended P-R is also 1, with the B-R range between 0.20 and 0.30.

From the results of investigating the installation of MVOs in the CHET under turbulent flow conditions with Reynolds numbers in the range of 3,000–16000, where the blockage ratio (B-R) was varied between 0.05 and 0.30, the pitch ratio (P-R) between 1–2, and the attack angles were 30°, 45°, and 60° in both + x and–x flow directions, the findings were analyzed to develop correlation equations. Equations 14–19 represent correlations for Nu/Nu_0, while Equations 20–25 represent correlations for f/f_0. The parameter Nu/Nu_0 is expressed as a function of Re, Pr, B-R, and P-R, whereas f/f_0 is expressed as a function of Re, B-R, and P-R. These developed correlation equations are intended to serve as guidelines for designing MVOs for practical applications in industrial or real operating systems.

$$Nu/Nu_0 = 96.752\mathrm{Re}^{-0.226}\,\mathrm{Pr}^{0.4}\,(B-R)^{0.503}\,(\mathrm{P\text{-}R})^{-0.323}, 30^o, +x \quad (14)$$

$$Nu/Nu_0 = 87.628\mathrm{Re}^{-0.231}\,\mathrm{Pr}^{0.4}\,(B-R)^{0.478}\,(P-R)^{-0.268}, 30^o, -x \quad (15)$$

$$Nu/Nu_0 = 141.638\mathrm{Re}^{-0.222}\,\mathrm{Pr}^{0.4}\,(B-R)^{0.618}\,(P-R)^{-0.357}, 45^o, +x \quad (16)$$

$$Nu/Nu_0 = 117.321\mathrm{Re}^{-0.217}\,\mathrm{Pr}^{0.4}\,(B-R)^{0.594}\,(P-R)^{-0.328}, 45^o, -x \quad (17)$$

$$Nu/Nu_0 = 182.409\mathrm{Re}^{-0.224}\,\mathrm{Pr}^{0.4}\,(B-R)^{0.696}\,(P-R)^{-0.396}, 60^o, +x \quad (18)$$

$$Nu/Nu_0 = 169.179\mathrm{Re}^{-0.242}\,\mathrm{Pr}^{0.4}\,(B-R)^{0.645}\,(P-R)^{-0.292}, 60^o, -x \quad (19)$$

$$f/f_0 = 79.630\mathrm{Re}^{0.176}\,(B-R)^{1.639}\,(P-R)^{-0.770}, 30^o, +x \quad (20)$$

$$f/f_0 = 57.705\mathrm{Re}^{0.198}\,(B-R)^{1.590}\,(P-R)^{-0.754}, 30^o, -x \quad (21)$$

$$f/f_0 = 235.132\mathrm{Re}^{0.210}\,(B-R)^{1.872}\,(P-R)^{-0.854}, 45^o, +x \quad (22)$$

$$f/f_0 = 221.630\mathrm{Re}^{0.173}\,(B-R)^{1.746}\,(P-R)^{-0.773}, 45^o, -x \quad (23)$$

$$f/f_0 = 420.505\mathrm{Re}^{0.226}\,(B-R)^{2.052}\,(P-R)^{-0.934}, 60^o, +x \quad (24)$$

$$f/f_0 = 307.622\mathrm{Re}^{0.196}\,(B-R)^{1.828}\,(P-R)^{-0.769}, 60^o, -x \quad (25)$$

Valid for air, Re = 3,000–16000, 0.05 ≤ B-R ≤ 0.30, 1 ≤ P-R ≤ 2.

When the values obtained from the correlations were compared with those from the simulations for both Nu/Nu_0 and f/f_0, as illustrated in Figures 11a,b, respectively, the maximum errors were found to be within 10% for Nu/Nu_0 and 15% for f/f_0.

7 Conclusion

This study presents the investigation of airflow dynamics and HT in the CHET using a passive technique to enhance HT. The effects of key parameters on both HT and flow behavior were examined, including blockage ratio (B-R = 0.05–0.30), pitch ratio (P-R = 1, 1.5, and 2), and attack angles of 30°, 45°, and 60°, under turbulent flow conditions corresponding to Reynolds numbers ranging from 3,000 to 16,000. Based on the analysis, the main findings can be summarized as follows:

The installation of MVO in the CHET directly alters the flow structure, inducing vortex formation due to flow obstruction and the resulting pressure drop across the MVO. These vortices significantly influence the thermal behavior by enhancing the mixing quality of fluids at different temperatures and by disturbing the regions in contact with the HT surface. The boundary-layer disturbance increases the convective HT coefficient, which is directly correlated with the HT rate and the Nusselt number.

The HT rate and pressure drop increase with increasing B-R and decreasing P-R, corresponding to the changes in vortex strength. An attack angle of 60° yields the highest HT rate and pressure drop, while an attack angle of 45° provides higher values than 30°. The + x flow direction results in greater HT rates and pressure drops compared to the–x direction. The maximum HT enhancement, 9.93 times that of the plain CHET, is observed at an attack angle of 60°. Meanwhile, the highest TEF of 1.92 occurs at an attack angle of 30°, P-R = 1, B-R = 0.25, in the +x flow direction.

For practical industrial applications, it is recommended to select the case that provides the highest TEF value, which should be greater than 1. For systems in which pressure drop is not a critical concern—such as certain types of dryers—the appropriate case can be chosen based solely on the one that yields the highest Nusselt number ratio.

When compared with previous studies, the present study demonstrates higher heat transfer rates than the circular ring (Kongkaitpaiboon et al., 2010b) and V-orifice (Jedsadaratanachai and Boonloi, 2017). In this study, the Nu/Nu_0 ratio reaches 9.93, whereas the circular ring (Kongkaitpaiboon et al., 2010b) and V-orifice (Jedsadaratanachai and Boonloi, 2017) yield 2.6 and 8.26, respectively. This indicates that the current design significantly enhances convective heat transfer due to more effective flow disruption and vortex generation. Regarding the thermal enhancement factor (TEF), the present study achieves a maximum TEF of 1.92, which is lower than the maximum TEF of 2.25 reported for the V-orifice (Jedsadaratanachai and Boonloi, 2017), but higher than that of the circular ring (Kongkaitpaiboon et al., 2010b), which has a maximum TEF of only 1.07. This suggests that while the V-orifice provides slightly better overall thermal performance when accounting for pressure drop, the present configuration offers a balanced improvement in heat transfer efficiency relative to pumping power, outperforming the circular ring significantly.

Data availability statement

The raw data supporting the conclusions of this article will be made available by the authors, without undue reservation.

Author contributions

AB: Resources, Writing – original draft, Investigation, Software, Funding acquisition, Visualization, Conceptualization, Formal Analysis, Validation, Data curation, Writing – review and editing, Methodology, Project administration, Supervision. WJ: Project administration, Resources, Validation, Visualization, Methodology, Conceptualization, Data curation, Formal Analysis, Investigation, Supervision, Funding acquisition, Writing – review and editing, Software, Writing – original draft.

Funding

The author(s) declared that financial support was received for this work and/or its publication. This research was funded by King Mongkut's University of Technology North Bangkok, Contract no. KMUTNB-69-KNOW-07.

Acknowledgements

The authors would like to thank Prof. Dr. Pongjet Promvonge for suggestions.

Conflict of interest

The author(s) declared that this work was conducted in the absence of any commercial or financial relationships that could be construed as a potential conflict of interest.

Generative AI statement

The author(s) declared that generative AI was not used in the creation of this manuscript.

Any alternative text (alt text) provided alongside figures in this article has been generated by Frontiers with the support of artificial intelligence and reasonable efforts have been made to ensure accuracy, including review by the authors wherever possible. If you identify any issues, please contact us.

Publisher's note

All claims expressed in this article are solely those of the authors and do not necessarily represent those of their affiliated organizations, or those of the publisher, the editors and the reviewers. Any product that may be evaluated in this article, or claim that may be made by its manufacturer, is not guaranteed or endorsed by the publisher.

References

Abajja, K. M. A., Selimli, S., Shaneb, A. M. A., and Eljetlawi, I. A. M. (2023). Enhancing heat transfer for laminar flow in heat pipes using perforated and jagged-edged twisted tapes: an experimental study. *Energy* 325 (15 June 2025), 136141. doi:10.1016/j.energy.2025.136141

Alqaed, S., Mustafa, J., and Sharifpur, M. (2024). Numerical and optimization study of turbulent water-copper nanofluid flow in a heat exchanger in power plant with conical rings: investigating conical ring hole diameter's influence. *Ann. Nucl. Energy* 203, 110494. doi:10.1016/j.anucene.2024.110494

Anvari, A. R., Lotfi, R., Rashidi, A. M., and Sattari, S. (2011). Experimental research on heat transfer of water in tubes with conical ring inserts in transient regime. *Int. Commun. Heat Mass Transf.* 38 (5), 668–671. doi:10.1016/j.icheatmasstransfer.2011.03.016

Anvari, A. R., Javaherdeh, K., Emami-Meibodi, M., and Rashidi, A. M. (2014). Numerical and experimental investigation of heat transfer behavior in a round tube with the special conical ring inserts. *Energy Convers. Manag.* 88, 214–217. doi:10.1016/j.enconman.2014.08.030

Bennour, E., Kaid, N., and Kezrane, C. (2025). Numerical investigation of improved mixing and heat transfer of a shear-thinning fluid in corrugated and baffled tube systems. *Appl. Therm. Eng.* 268 (1 June 2025), 125863. doi:10.1016/j.applthermaleng.2025.125863

Bhattacharyya, S., Vishwakarma, D. K., and Soni, M. K. (2025). Experimental investigation of twisted tape-induced mixed convection for optimized thermofluidic performance in transitional flow regimes. *Int. Commun. Heat Mass Transf.* 164 (Part A), 108865. doi:10.1016/j.icheatmasstransfer.2025.108865

Bizuneh, Y. E., Kassie, T. D., Gebresilassie, E. B., and Bizuneh, A. E. (2025). Numerical investigation on heat transfer of CuO-water nano-fluid in a circular pipe with twisted tape inserts. *Int. J. Thermofluids* 27, 101260. doi:10.1016/j.ijft.2025.101260

Cengel, Y. A., and Ghajar, A. J. (2015). Heat and mass transfer: fundamentals and applications. in *SI units*. Fifth edition (McGraw-Hill Education).

Feng, J. J., Teh, C. P., Ng, K. C., Jen-Haw, J. C., Xiao, D., Abakr, Y. A., et al. (2024). Heat transfer and fluid flow analysis in circular tubes with multi-delta-winglets vortex generators. *Int. Commun. Heat Mass Transf.* 159 (Part C), 108267. doi:10.1016/j.icheatmasstransfer.2024.108267

Ghazanfari, V., Mansourzade, F., Taheri, A., Amini, Y., and Shadman, M. M. (2025). Enhancing thermal efficiency in helical heat exchangers: a CFD study on twisted tube configurations. *Case Stud. Therm. Eng.* 73, 106694. doi:10.1016/j.csite.2025.106694

Hassan, M. A., Al-Tohamy, A. H., and Kaood, A. (2022). Hydrothermal characteristics of turbulent flow in a tube with solid and perforated conical rings. *Int. Commun. Heat Mass Transf.* 134, 106000. doi:10.1016/j.icheatmasstransfer.2022.106000

Ibrahim, M. M., Essa, M. A., and Mostafa, N. H. (2019). A computational study of heat transfer analysis for a circular tube with conical ring turbulators. *Int. J. Therm. Sci.* 137, 138–160. doi:10.1016/j.ijthermalsci.2018.10.028

İğcï, A. A. (2025). Enhancing heat transfer with a hybrid Vortex generator combining delta wing and winglet designs: a numerical study using the GEKO turbulence model. *Appl. Therm. Eng.* 258 (Part A), 124604. doi:10.1016/j.applthermaleng.2024.124604

Jedsadaratanachai, W., and Boonloi, A. (2017). Numerical study on turbulent forced convection and heat transfer characteristic in a circular tube with V-Orifice. *Model. Simul. Eng.* 2017, 1–20. doi:10.1155/2017/3816739

Kongkaitpaiboon, V., Nanan, K., and Eiamsa-ard, S. (2010a). Experimental investigation of heat transfer and turbulent flow friction in a tube fitted with perforated conical-rings. *Int. Commun. Heat Mass Transf.* 37 (5), 560–567. doi:10.1016/j.icheatmasstransfer.2009.12.015

Kongkaitpaiboon, V., Nanan, K., and Eiamsa-Ard, S. (2010b). Experimental investigation of convective heat transfer and pressure loss in a round tube fitted with circular-ring turbulators. *Int. Commun. Heat Mass Transf.* 37, 568–574. doi:10.1016/j.icheatmasstransfer.2009.12.016

Kumar, J., and Afzal, M. S. (2025). Performance evaluation of a double-pipe heat exchanger using plain and rectangular-cut multi-channel twisted tapes. *Int. J. Therm. Sci.* 215, 109994. doi:10.1016/j.ijthermalsci.2025.109994

Kumar, N., Kumar, A., and Maithani, R. (2020). Development of new correlations for heat transfer and pressure loss due to internal conical ring obstacles in an impinging jet solar air heater passage. *Therm. Sci. Eng. Prog.* 17 (1 June 2020), 100493. doi:10.1016/j.tsep.2020.100493

Kumar, A., Ali, M. A., Maithani, R., Kumar Gupta, N., Sharma, S., Kumar, S., et al. (2023). Experimental analysis of heat exchanger using perforated conical rings, twisted tape inserts and CuO/H_2O nanofluids. *Case Stud. Therm. Eng.* 49, 103255. doi:10.1016/j.csite.2023.103255

Li, J., E, J., Ding, J., Cai, L., and Luo, B. (2024). Numerical investigation of inserting conical ring into the micro-combustor with premixed hydrogen/air to enhance the heat transfer performance for the micro-thermophotovoltaic system. *Int. J. Hydrogen Energy* 69, 51–67. doi:10.1016/j.ijhydene.2024.04.348

Li, Y., Lei, Y., Li, J., Du, B., Song, C., and Wang, Y. (2025). Experimental investigation on the thermo-hydraulic performance and entransy analysis of a shell-and-tube heat exchanger with louver baffles. *Appl. Therm. Eng.* 269, 125928. doi:10.1016/j.applthermaleng.2025.125928

Majmader, F. B., and Hasan, M. J. (2024). Multi-objective hydrothermal performance optimization of a microchannel heat sink equipped with delta winglet vortex generators using NSGA-II genetic algorithm. *Int. J. Therm. Sci.* 201, 109046. doi:10.1016/j.ijthermalsci.2024.109046

Mohammed, H. A., Abuobeida, I. A. M. A., Vuthaluru, H. B., and Liu, S. (2019). Two-phase forced convection of nanofluids flow in circular tubes using convergent and divergent conical rings inserts. *Int. Commun. Heat Mass Transf.* 101, 10–20. doi:10.1016/j.icheatmasstransfer.2018.12.010

Nakhchi, M. E., and Esfahani, J. A. (2019a). Numerical investigation of turbulent Cu-water nanofluid in heat exchanger tube equipped with perforated conical rings. *Adv. Powder Technol.* 30 (7), 1338–1347. doi:10.1016/j.apt.2019.04.009

Nakhchi, M. E., and Esfahani, J. A. (2019b). Numerical investigation of different geometrical parameters of perforated conical rings on flow structure and heat transfer in heat exchangers. *Appl. Therm. Eng.* 156 (25 June 2019), 494–505. doi:10.1016/j.applthermaleng.2019.04.067

Rinik, R. A., Bhuiyan, A. A., and Karim, M. R. (2025). Enhancement of heat transfer using elliptical twisted inner pipe with convergent conical ring turbulator for turbulent

flow in double pipe heat exchanger. *Int. J. Therm. Sci.* 210, 109558. doi:10.1016/j.ijthermalsci.2024.109558

Saini, P., Dhar, A., and Powar, S. (2024a). Performance evaluation of a parabolic trough collector with a uniform helical wire coil flow insert. *Results Eng.* 21, 101794. doi:10.1016/j.rineng.2024.101794

Saini, P., Dhar, A., and Powar, S. (2024b). Effect of the X-grid static mixer flow inserts on the performance of parabolic trough collector. *Int. J. Thermofluids* 21, 100544. doi:10.1016/j.ijft.2023.100544

Salhi, J. E., Zarrouk, T., Alam, T., Siddiqui, M. I. H., Dobrotă, D., and Mumtaz, M. A. (2025). Three-dimensional analysis of thermohydraulic performance in corrugated channels with embedded baffles: optimization of heat transfer and energy efficiency. *Case Stud. Therm. Eng.* 69 (May 2025), 106019. doi:10.1016/j.csite.2025.106019

Sheikholeslami, M., Ganji, D. D., and Gorji-Bandpy, M. (2016). Experimental and numerical analysis for effects of using conical ring on turbulent flow and heat transfer in a double pipe air to water heat exchanger. *Appl. Therm. Eng.* 100 (5 May 2016), 805–819. doi:10.1016/j.applthermaleng.2016.02.075

Sripattanapipat, S., Tamna, S., Jayranaiwachira, N., and Promvonge, P. (2016). Numerical heat transfer investigation in a heat exchanger tube with hexagonal conical-ring inserts. *Energy Procedia* 100, 522–525. doi:10.1016/j.egypro.2016.10.213

Suchatawat, M., Sripattanapipat, S., Promthaisong, P., Skullong, S., and Promvonge, P. (2025). Enhanced thermal performance in solar receiver duct with louver-punched V-type winglets: numerical and experimental study. *Results Eng.* 25 (March 2025), 103702. doi:10.1016/j.rineng.2024.103702

Tian, Z., Zhang, Y., Xiong, X., Gou, G., and Wu, Y. (2024). Performance enhancement of high temperature fin-and-tube heat exchanger employing winglet combined vortex generators. *Appl. Therm. Eng.* 249 (15 July 2024), 123376. doi:10.1016/j.applthermaleng.2024.123376

V P, C., Bakthavatchalam, B., Jayakumar, V., Kusekar, S., Pandey, A. K., Habib, K., et al. (2025). Enhancing heat transfer in compound twisted square ducts using shortened twisted tape inserts. *Results Eng.* 26, 104862. doi:10.1016/j.rineng.2025.104862

Wang, C., Sun, Y., Wang, N., Sun, J., and Yue, Y. (2025). Study on the influence of baffles on heat transfer characteristics of particles in an oil shale rotary kiln. *Appl. Therm. Eng.* 268 (1 June 2025), 125924. doi:10.1016/j.applthermaleng.2025.125924

Zhan, Y., Zhang, H., and Zhang, S. (2025). Numerical investigation of flow and heat transfer characteristics in a rectangular channel with perforated inclined baffle. *Int. Commun. Heat Mass Transf.* 164, 108941. doi:10.1016/j.icheatmasstransfer.2025.108941

Zhang, B., Yang, Y., and Wu, Y. (2025). Study on the performance of a novel sinusoidal staggered shell and tube heat exchanger without baffle with experiment verification and CFD modeling. *J. Energy Storage* 114, 115832. doi:10.1016/j.est.2025.115832

Glossary

b MVO thickness, m

C_μ constant value (=0.0845)

D tube diameter, m

f friction factor, friction loss

h convective HT coefficient, W m^{-2} K^{-1}

k turbulent kinetic energy, $k = (\overline{u_i' u_i'})/2$

k_t thermal conductivity, W m^{-1} K^{-1}

L numerical model length/periodic length

Nu Nusselt number

p static pressure, Pa

P pitch spacing, m

Pr Prandtl number

Re Reynolds number

T fluid temperature, K

$\bar{u}$ fluid mean velocity in square duct, m s^{-1}

u_i mean component of velocity in the direction x_i, m s^{-1}

u' fluctuating component of velocity, m s^{-1}

Greek symbol

α attack angle, deg

ρ density, kg m^{-3}

μ dynamic viscosity, kg $m^{-1}s^{-1}$

μ_{eff} effective viscosity

μ_t turbulent viscosity, $\mu_t = \rho C_\mu k^2/\varepsilon$

α_k inverse effective Prandtl number for k

α_ε inverse effective Prandtl number for ε

Γ molecular thermal diffusivity

Γ_t turbulent thermal diffusivity

δ_{ij} a Kronecker delta

Subscripts

0 smooth tube

pp driving force

Abbreviations

B-R flow blockage ratio

CHET circular heat exchanger tube

HT heat transfer

MVO modified V-orifice

P-R pitch ratio

TEF thermal enhancement factor $(=(Nu/Nu_0)/(f/f_0)^{1/3})$

VF vortex flow